



Removing of Cr(III) and Cr(VI) compounds from aqueous solutions by shale waste rocks

Beata Jabłońska

Czestochowa University of Technology, Faculty of Infrastructure and Environment, Department of Environmental Engineering, Brzeźnicka St. 60a, 42-200 Czestochowa, Poland, Tel. +48 34 32 50 917; email: beata.jablonska@pcz.pl

Received 26 September 2019; Accepted 3 January 2020

ABSTRACT

Shale is a sedimentary rock often occurring in gangue that accompanies coal and other minerals. It is extracted with them and often treated as waste rock. In the paper, the shale was tested for sorption of Cr(III) and Cr(VI) ions from aqueous solutions. The samples were taken from three different Polish mines. The structural and surface properties of the shales were determined via nitrogen adsorption/desorption. The specific surface area of the shales ranges from 10.3 to 12.3 m²/g. In sorption tests, the effect of pH was tested. The initial concentrations of chromium ions fell in range 1–500 mg/L for Cr(III) and 1–100 mg/L for Cr(VI). Several adsorption models were considered. The adsorption follows the Langmuir isotherm. The sorption capacity in the Langmuir model is 7.67–9.85 mg/g for Cr(III), whereas only 0.56–4.66 mg/g for Cr(VI). The sorption percentage equals 75%–90% for low concentrations of chromium ions, and drops with an increase in the initial concentration. There is a significant difference between the tested shales in chromium sorption, especially for Cr(VI). One of the tested shales turned out to have best performance for both Cr(III) and Cr(VI).

Keywords: Shale; Chromium sorption; Structural properties

1. Introduction

An important contemporary problem of water and soil environments is the constantly growing pollution with chromium compounds. In 2019, about 36,000 Mg of chromium ore were extracted and processed in the world. The largest known chromium resources (95%) are located in Kazakhstan and South Africa; in addition, smaller but still significant amounts of chromium are also in the United States, Turkey, India and some other countries [1]. The main chromium sources used in the industry are ores containing chromite (FeCrO) and krokoite (PbCrO) [2]. The world's resources of chromite are assessed to over 12 billion tons [1]. Chromium compounds are used in various branches of industry, among others for the production of high-quality steel as the main alloy addition, in galvanization, tanning, in the textile industry, for the production of paints, plastics

and dyes [3]. For example, China is a leading country using ferro-chromium to produce stainless steel [1]. Chromium ore extraction and industrial activity contributes to the generation of large amounts of waste and chromium wastewater. The accumulation of metals in soils increases over time, and is the result of not only mining activities, but also minerals containing metals, geographical features and even the local dominant wind in the area [4]. The presence of chromium in the environment is a potential threat to aquatic animals and humans, because, among others, may lead to skin sensitivity and greater likelihood of genetic defects, including cancer [5].

Chromium is present in several oxidation states; in aqueous solutions it is mainly +3 and +6, rarely +2 [6]. Cr(VI) is much more toxic than Cr(III) because it has a greater ability to penetrate cell membranes. According to the classification by International Agency for Research on Cancer (IARC), Cr(VI) belongs to particularly dangerous compounds [7].

Cr(III), on the other hand, is 300 times less toxic than Cr(VI) because it has limited solubility in hydroxide, which makes it less mobile and bioavailable in the environment [8].

The harmful effect of chromium compounds and their migration in the water-ground environment forces the search for more effective and ecologically safe ways of their removal from sewage and water. The most commonly used methods for the treatment of wastewater containing chromium are precipitation methods [9], ion exchange [10], membrane processes [11], electrochemical methods [12] and adsorption [13]. As given in [14], the precipitation methods are technologically simple and not very expensive, however they require chemicals, produce sludge and the efficiency is best for higher concentrations of pollutant. The ion exchange methods are simple and efficient, but very expensive and susceptible to other pollutants, saturation and blocking. Similar features can be attributed to membrane processes. The electrochemical methods are also very expensive, produce sludge and require additional processes like filtration and post-treating to remove iron and aluminum ions. The processes often involve the generation of harmful secondary pollutants (sub-process waste), their efficiency is diversified, the costs associated with the development of a technological system for wastewater treatment is usually high, and they are frequently unprofitable in the case of wastewater treatment where the concentration of metal does not exceed 100 mg/L [15,16]. As for adsorption, usually the most effective are specialized synthetic substances, like activated carbons [17,18], ion exchange resins [19], synthetic zeolites [20,21], or chitosan-based adsorbents [22,23]. Their disadvantage is considerable manufacturing cost; therefore, there is a constant search for inexpensive adsorbents that could be used in purifying or pre-treating wastewater from chromium compounds. Among them there are many bio-adsorbents (e.g. wool, olive cake, sawdust, pine needles, almond shells, cactus leaves, charcoal [24]; jackfruit leaf, mango leaf, onion peel, garlic peel, bamboo leaf, acid treated rubber leaf, coconut shell powder [25] and many others [15,16]), waste materials (e.g. newspapers [26], fly ash [27]) and natural minerals (e.g. zeolites [21,28], vesicular basalt rock [29,30], volcanic rocks [31], kaolinite [32], montmorillonite [33], clay [34], kaolin [35], palygorskite clay [36], bentonite [37]). One of such natural minerals is Carboniferous coal shale included in the so-called gangue, which is a rock accompanying the hard coal deposit. It occurs in the form of interbeddings (so-called overgrowths) in coal seams of many coal basins all over the world [38]. The largest amount of gangue is extracted by hard coal mines in China, annually about 300–350 million Mg [39]. According to the Central Statistical Office in Poland, over 63 million Mg of waste from the extraction of minerals other than metal ores were created in 2018 [40]. This material is often deposited in the form of spoil tips, but a part of it is managed in various ways. In Poland, the gangue is mainly used for hardening roads and yards as well as in the process of reclamation of degraded areas (about 47% of managed waste) [41,42]. In the world it is also used for the production of geopolymers, bricks, cement, for energy production and in agriculture as a fertilizer [38,43]. Post-mining wastes were also tested with respect to structural properties [44] and proposed as inexpensive phenol adsorbent [45]. The shale is an easily available mineral waste material, the cost

of which is much lower than in the case of ion exchangers or filtration membranes. In addition to its use in wastewater treatment, this material may be a fill of mineral (sorption) barriers that immobilize chromium compounds. Such a use of mineral wastes will partially help to solve the problem of their management, being a part of clean production as one of the key strategies in achieving sustainable development.

The purpose of the work is to determine the possibility of using natural shale as low-cost adsorbent, by characterizing its most important structural and surface parameters determining sorption properties and assessing the sorption capacity of shale with respect to Cr(III) and Cr(VI) compounds.

2. Materials and methods

2.1. Materials

The research involved the use of shales, which were taken from three hard coal mines located in the Upper Silesian Coal Basin (USCB) in Poland. The coal mine 1 (CM1) produces coal in the south-eastern part of the USCB, whereas the two other mines (CM2 and CM3) operate in the northern part of the USCB in the Upper Carboniferous formations. The Upper Carboniferous deposits are composed of coal seams interbedded alternately with rocks: siltstones, claystones, shales and sandstones [46]. In the mines, the shales are classified as gangue, which is a mineral waste formed during the preparation of hard coal deposits for exploitation. For the research, several samples of rocks were ground to a grain size below 0.2 mm, and dried to air-dry state.

The rocks in their natural state have a gray color due to the presence of a strongly dispersed amorphous carbonaceous substance. The analyzed samples are characterized by a high content of clay minerals. The mineralogical composition of shales was identified on earlier stage of research [47]. The main clay minerals present in their composition are illites, kaolinites together with chlorites, quartz and hematite admixtures. The chemical composition (X-ray fluorescence spectrometry (XRF) on a PW 1404 spectrometer, Philips) and the loss on ignition (LOI) (determination as given in [48]) of the examined rocks is presented in Table 1; it reflects their mineral composition.

In the chemical composition, the main components of the studied shales are SiO_2 , Al_2O_3 and K_2O , the amount of which is related to the presence of quartz, kaolinite and illite in the mineral composition. The highest content of K_2O in the rocks examined is in the sample CM2 (3.3%), and the lowest in CM1 (2.83%). Its presence is also the reason for lower LOI in this sample (Table 1), because unlike other clay minerals (e.g. montmorillonite, halloysite, vermiculite) illite does not contain interpacket water. The Na_2O content is related to the presence of feldspars and micas in the tested samples (the highest in CM2 – 0.51%). The Fe_2O_3 content is related to the presence of hematite in the studied rocks and also has a significant share in their chemical composition. The amounts of trace elements (inductively coupled plasma emission spectrometer ICP-ASA, Thermo) complement the total chemical composition of the studied rocks (Table 2). The content of the metals was compared with their permissible contents in soils and surface soils (at a depth of 0–0.3 m) given in [49]. It follows that values are below the permissible values.

Table 1
Chemical composition of the studied shales

	Content, dry mass %											
	SiO ₂	TiO ₂	Al ₂ O ₃	Fe ₂ O ₃	CaO	MgO	Na ₂ O	K ₂ O	P ₂ O ₅	SO ₃	MnO	LOI
CM1	54.9	0.97	21.7	5.4	1.1	2.15	0.26	2.83	0.09	0.12	0.01	9.86
CM2	58.6	1.03	19.9	6.15	0.29	2.02	0.51	3.3	0.08	0.17	0.06	7.2
CM3	60.3	1.02	21.9	4.38	0.55	1.84	0.35	2.9	0.08	0.22	0.05	5.9

Note: LOI is loss on ignition

Table 2
The content of trace elements in the examined shales and the permissible contents of these metals in B group lands

Sample	Element content, mg/kg d.m.											
	As	Ba	Cd	Co	Cr	Cu	Hg	Mo	Ni	Pb	Sn	Zn
CM1	11	119.4	<1	5.5	34.4	43.9	<1	<2	18.9	<2	<2	169
CM2	<2	82.9	3	15.3	59.9	42.9	0.04	<2	48.7	26	2	91.3
CM3	<2	125	<2	10	55.8	14.3	<1	<2	47.2	56	<2	128.3
Permissible	20	200	4	20	150	150	2	10	100	100	20	300

Note: B group land - land classified as agricultural land, forest land as well as wooded and shrubby land, built-up and urbanized land, excluding industrial areas.

2.2. Structural properties

The structural properties of the materials tested were determined based on nitrogen adsorption/desorption (−196°C) in the range of relative pressures from about 0.01 to 0.995 (AutosorbiQ, Quantachrome Instruments, US). The samples were degassed at 150°C for 6–30 h at 10^{−4} mmHg before the measurement.

Based on the isotherms, the specific surface area, pore volume distribution, and fractal dimension were determined. The specific surface area was determined based on modified Brunauer–Emmett–Teller (BET) equation [50], whose linearized form is given by Eq. (1) as follows:

$$\frac{x[1-x^n - nx^n(1-x)]}{v(1-x)^2} = \frac{1}{v_m C} + \frac{1}{v_m} \frac{x(1-x^n)}{1-x} \quad (1)$$

where x is the relative pressure of nitrogen vapor, v - volume of adsorbed nitrogen at standard temperature and pressure (STP) (cm³/g), v_m - monolayer volume (cm³/g at STP), C - a positive dimensionless constant, and n - number of layers accessible for adsorption (not necessarily an integer value). In calculations, n was varied in range 2–5 and then v_m and C were determined from the above equation via linear regression. Then R^2 (the coefficient of determination) was calculated, and the final results were assumed those for which R^2 was closest to 1. Then the BET surface area, S_{BET} was calculated according to [50] using Eq. (2) as follows:

$$S_{\text{BET}} = 4.35 \times v_m \left[\frac{\text{m}^2}{\text{g}} \right] \quad (2)$$

The pore size distribution was determined via Barrett–Joyner–Halenda (BJH) analysis under the assumption of

cylindrical shape of the pores, using the Kelvin equation for meniscus radius corresponding to the relative pressure, and using the standard Harkins–Jura statistical thickness of the adsorbate layer.

The microporosity analysis was performed using the Dubinin–Radushkevich (DR) theory [50] using Eq. (3) as follows:

$$\frac{V_{\text{mic}}}{V_0} = \exp \left[-K_{\text{DR}} \left(RT \ln \frac{1}{x} \right)^2 \right] \quad (3)$$

where V_0 is the total volume of micropores (mm³/g), V_{mic} - the volume of micropores (mm³/g) filled at relative pressure x , R - gas constant (8.314 J/(mol K)), T - temperature (K), K_{DR} - constant related with mean free energy of adsorbent-adsorbate system.

The fractal dimension (D) was calculated according to [51] by linear regression of the nitrogen adsorption/desorption data via Eq. (4) as follows:

$$\ln \left[-\frac{1}{r_K^2} \int_{v(x)}^{v_{\text{max}}} \ln x \, dv \right] = \text{const} + D \ln \frac{(v_{\text{max}} - v)^{1/3}}{r_K} \quad (4)$$

where v is the volume of adsorbed nitrogen (cm³/g at STP) at relative pressure x , v_{max} - the maximum volume of adsorbed nitrogen, and r_K is the Kelvin radius corresponding to the relative pressure x . In the above equation, the range of relative pressure was 0.4–0.99.

2.3. Zero point of charge pH determination

The zero point of charge pH (pH_{zpc}) was determined using the constant addition method according to [52]. First,

a 0.01 mol/L NaCl solution was prepared. Then 50 ml of NaCl solution were added to a series of polyethylene bottles of a capacity of 200 ml, and pH was adjusted in the range from 2 to 11 using 0.1 mol/L HCl or 0.1 mol/L NaOH. After 2 h of equilibration, the initial pH (pH_{init}) was determined. Then 0.15 g of adsorbent was added to each bottle, each sample was flushed with nitrogen and capped. The samples were shaken at room temperature for 24 h at 200 rpm. After 72 h, the final pH (pH_{fin}) was measured using a pH meter (Elmetron CPC-401). The pH_{zpc} value was determined from a curve that intersects the initial pH axis in a ($pH_{init} - pH_{fin}$) vs. pH_{init} plot.

2.4. Sorption tests

Sorption tests were carried out using the static batch method from mono-component synthetic solutions prepared based on chemical compounds of Cr(III) and Cr(VI) with initial concentrations comparable to those found in industrial wastewater. Cr(III) solutions were prepared from chromic nitrate $Cr(NO_3)_3 \cdot 9H_2O$, and Cr(VI) from potassium dichromate $K_2Cr_2O_7$. The tests of Cr(III) and Cr(VI) adsorption from aqueous solutions were made in suspensions with shale concentration of 2% (4 g of mineral sediment was added to 0.2 L aqueous solutions). The initial concentrations ranged from 1 to 500 mg/L for Cr(III) and from 1 to 100 mg/L for Cr(VI). The samples were shaken in flasks on an Elpin Plus 358A shaker at 20°C for 4 h, and then they were left for 20 h in a dark room (the total contact time was 24 h). Next, the aqueous solution was decanted and centrifuged on an Equimet MPW-223 centrifuge at a speed of 2500 rpm to remove the shale from the solution.

When assessing the effect of Cr(VI) concentration on its sorption, the suspension was shaken under conditions caused by the natural pH of the sorbent and the acid pH of the added chromium solutions. However, due to the ability of Cr(VI) binding by the waste rocks is a result of its instability at low pH; therefore, the sorption studies of Cr(VI) were carried out at pH = 5. It was set at the same level for all solutions. The Cr(III) sorption was performed in an analogous manner, with the pH of the initial solutions being 4.

When assessing the effect of pH on the chromium sorption, the shale sample (4 g) was mixed with solutions of concentrations 5 mg/L for Cr(VI) and 100 mg/L for Cr(III), added 0.1 M HCl or 0.1 M NaOH to obtain the initial pH in the range from 1 to 11, and shaken for 4 h. Three series of measurements were carried out for each sample, and in the following considerations average values were considered.

The equilibrium concentration of Cr(VI) was determined by the colorimetric method with diphenylcarbazide using a HELIOS α Spectrophotometer (Thermo Electron Corporation, US) at 540 nm [53]. The equilibrium concentration of Cr(III) was performed on an inductively coupled plasma emission spectrometer (ICP-ASA, Thermo Fisher Scientific, US).

The amount of adsorbed Cr(III) and Cr(VI), q (mg/g), was calculated using Eq. (5) as follows:

$$q = \frac{C_i - C_e}{m} V \quad (5)$$

where C_i is the initial concentration (mg/L), C_e is the equilibrium concentration (mg/L), V is the volume of the solution (L), and m is the mass of adsorbent (g).

In the description of adsorption of Cr(III) and Cr(VI), the Freundlich, Langmuir, Langmuir–Freundlich, Elovich, Temkin and Dubinin-Radushkevich (DR) adsorption isotherms were used. They establish a relation between the amount of adsorbed substance (mass of adsorbate per unit mass of the adsorbent, q , mg/g), and the adsorbate concentration in the fluid in equilibrium (C_e , mg/L). The Freundlich isotherm [54] has the form given by Eq. (6) as follows:

$$q = K_F C_e^{1/n_F} \quad (6)$$

where K_F and $n_F > 1$ are empirical constants depending on the adsorbent and adsorbate at a fixed temperature. The formula has a purely empirical character; nevertheless, it often fits the experimental data very good. Physically, it indicates heterogeneity of the adsorbent surface. The Freundlich isotherm constant, K_F , can be regarded as a measure of adsorption capacity, but it is worth emphasizing that parameters K_F for various n_F have different units and should not be compared directly. Parameter n_F is related with the intensity of adsorption: adsorption nearly proportional to C_e results in n_F nearly 1, whereas larger values of n_F cause the isotherms deviate downwards as C_e increases, which means the adsorption becomes weaker due to filling up the adsorption sites.

The Langmuir adsorption isotherm [54] is expressed by Eq. (7) as follows:

$$q = \frac{Q_L K_L C_e}{1 + K_L C_e} \quad (7)$$

where K_L and Q_L are constants for each pair of adsorbate and adsorbent at a given temperature. This equation is a result of monolayer adsorption model. Coefficient Q_L (mg/g) can be interpreted as the monolayer adsorption capacity, towards which q tends asymptotically for large C_e . In turn, the Langmuir adsorption constant, K_L (L/mg), is related with the intensity of adsorbate-adsorbent interaction. The greater the value of K_L the lower the concentration at which the saturation of the adsorbent occurs at a level of Q_L .

The Langmuir–Freundlich isotherm [55] has the following form given by Eq. (8):

$$q = \frac{Q_{LF} (K_{LF} C_e)^{n_{LF}}}{1 + (K_{LF} C_e)^{n_{LF}}} \quad (8)$$

where Q_{LF} , K_{LF} and n_{LF} are the Langmuir–Freundlich maximum adsorption capacity (g/mg), equilibrium constant (L/mg) and heterogeneous parameter, respectively. It is especially suitable for heterogeneous surfaces. For low concentrations it resembles the Freundlich isotherm, whereas for high concentrations it manifests saturation at a level of Q_{LF} .

The Elovich isotherm equation [54] has the form given by Eq. (9) as follows:

$$\frac{q}{Q_E} = K_E C_e \exp\left(-\frac{q}{Q_E}\right) \quad (9)$$

where Q_E (mg/g) is the Elovich maximum adsorption capacity, and K_E (L/mg) is the Elovich equilibrium constant. The Elovich isotherm assumes that the amount of adsorbate in equilibrium is proportional to C_e , but the proportionality coefficient decreases abruptly as the uptake increases.

The Temkin isotherm [54] can be expressed by Eq. (10) as follows:

$$q = K_T \ln(A_T C_e) \quad (10)$$

where K_T and A_T are empirical constants depending on the adsorbate and adsorbent. The coefficient K_T (mg/g) is related to heat of adsorption, whereas A_T (L/mg) is the equilibrium binding constant. The Temkin isotherm originates from the Langmuir one in which the heat of adsorption decreases linearly as the coverage of the surface accessible to adsorption increases.

To estimate the mean free energy in the solid/liquid system, the DR isotherm given by Eq. (3) was used, in which ratio V_{\min}/V_0 is replaced with q/Q_{DR} and $x = C_e/C_s$, where C_s is the solubility of adsorbate and Q_{DR} is interpreted as the sorption capacity [56]. The mean free energy was calculated according to Eq. (11):

$$E_{DR} = \frac{1}{\sqrt{2K_{DR}}} \quad (11)$$

where K_{DR} is the coefficient in Eq. (3).

In calculations, all parameters of all the isotherms were calculated using the least square method applied to nonlinear regression.

3. Results and discussion

3.1. Structural and surface properties

The structural and surface properties of the tested shales are characterized by parameters shown in Table 3.

The highest volume of pores filled at relative pressure 0.99 is obtained for CM1, but not much lower values were obtained for the other samples. The obtained values of the specific surface area of rocks in their natural state range from 10.34 m²/g for CM3 to 12.3 m²/g for CM2. A slightly smaller area (8.63 m²/g) was obtained for gangue taken from the Jiyuan region in the Henan province of China [57]. Also, similar surface values were noted for natural and acid-modified kaolinite, ranging from 3.8 to 15.6 m²/g [58]. The C-values for the samples tested are in the range from 50 to 150, which shows that the B point on the BET isotherm is quite well localized, and the obtained monolayer capacities are reliable [59]. The R² coefficient is close to one, showing almost perfect matching the BET isotherm to the data.

The results of the BJH analysis show that the dominant pores in the tested samples are mesopores with a diameter of ca. 3.9 nm. A similar value of the dominant pore diameter (3.8–4 nm) has natural gangue [44,57]. The percentages of mesopores in the rocks are from 8% for CM3, through 17% for CM1 to 31% for CM2 (Table 3). The average pore size (assuming a cylindrical shape) is the smallest for the CM2 (17 nm), the larger for the CM3 sample (28.4 nm) and by far the largest for CM1 (43.9 nm). Hence, the shale taken from CM2 contains many mesopores (Fig. 1), which translates into a larger specific surface area (12.3 m²/g). However, this principle did not

Table 3
Structural and surface properties of the tested shales from coal mines 1, 2 and 3

Parameter	CM1	CM2	CM3
Pore volume			
Total pore volume filled, mm ³ /g	210.9	107.4	149.4
Pore volume filled at $v = 0.99$, mm ³ /g	73.4	70.0	68.2
BET analysis			
Specific surface area S_{BET} , m ² /g	10.87	12.30	10.34
Monolayer volume v_m , cm ³ /g (STP)	2.50	2.82	2.38
Constant C in modified BET equation	150	57	62
Exponent n in modified BET equation	3.8	5.0	5.0
Determination coefficient R^2	1.0000	0.9998	0.9999
BJH analysis			
Dominant pore size, nm	3.9	3.9	3.9
Average pore size, nm	43.9	17.0	28.4
Accumulated pore volume, mm ³ /g	213.3	111.6	152.7
• macropores, mm ³ /g	194.3	74.2	127.2
• mesopores, mm ³ /g	17.2	35.5	23.4
• micropores (by subtraction), mm ³ /g	1.7	1.9	2.1
Other parameters			
Micropore volume by RD equation V_ν , mm ³ /g	4.12	4.18	3.62
Fractal dimension, D	2.21–2.30	2.55–2.54	2.31–2.37

work in the case of CM1 sample with the most macropores and the specific surface area slightly higher than that for the CM3 sample - this could be a result of presence of micropores. Indeed, the parameters of RD equation indicate that the volume of micropores in CM1 sample ($4.12 \text{ mm}^3/\text{g}$) is larger than in CM3 sample ($3.62 \text{ mm}^3/\text{g}$). Hence, the results correspond to the obtained surface area values (Table 3). The smallest fractal dimension was obtained for CM1 sample (2.21–2.30), and the largest one for CM2 sample (2.55–2.54), which confirms the highest degree of surface development of this sample.

3.2. Zero point of charge pH

Fig. 2 shows the pH_{zpc} results for the tested shales. The shales from CM1 and CM2 have very similar characteristics, and their $\text{pH}_{\text{zpc}} \approx 7$. The sample from CM3 is apparently different ($\text{pH}_{\text{zpc}} \approx 5$). Since Cr(VI) usually occurs in solutions in anionic forms, it can be expected that best sorption will be obtained for pH around 4–5, and it should be better on shales from CM1 and CM2. This is confirmed in sorption tests. As for Cr(III), which can occur mostly in cationic forms, the most desirable pH of the solution would be 8–10. However, at high values of pH Cr(III) tends to form hydroxide which is likely to precipitate. To avoid disturbances in adsorption tests due to that fact, the value of pH during sorption was much lower and equaled 4.

3.3. Effect of pH on Cr(III) and Cr(VI) sorption

The effect of pH on the adsorption of Cr(VI) and Cr(III) on the tested material is shown in Figs. 3 and 4. Adsorption

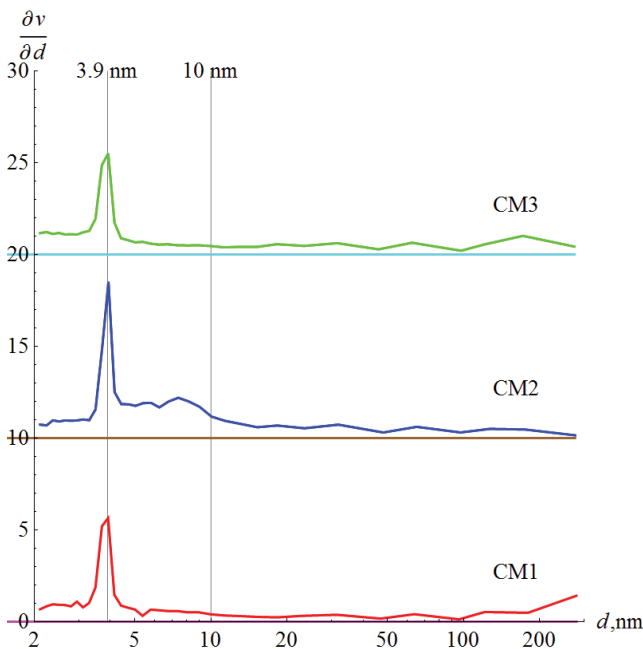


Fig. 1. Pore size distribution in the shales from coal mines 1, 2 and 3 according to BJH analysis (curves for CM2 and CM3 are shifted upwards by 10 and 20, respectively, to make the figure more legible); all curves reveal that the dominant pores diameter is 3.9 nm, and the curve for CM2 manifest a significant presence of mesopores.

of Cr(VI) is higher at lower pH. The maximum amount of chromium (89–99%) was adsorbed at pH 2–3. With an increase in pH to 5, it decreased to about 45% for CM2 and CM3 mines, and to 59% for CM1. A further increase in pH is accompanied by a gradual decrease in the amount of Cr(VI) adsorbed. The value of pH determines the process of adsorption of chromium compounds. This value strongly affects the ionic type of Cr(VI) present in water (H_2CrO_4 ; HCrO_4^- ; CrO_4^{2-} ; HCr_2O_7^- ; $\text{Cr}_2\text{O}_7^{2-}$) as well as the adsorbent surface charge sign [60]. With an increase in pH the degree of protonation of the adsorbent surface decreases, then negatively charged functional groups predominate in the solution [61]. In an acidic environment, the chromium species found in the solution are: H_2CrO_4 , HCrO_4^- and $\text{Cr}_2\text{O}_7^{2-}$, whereas CrO_4^{2-} ions predominate in the alkaline environment. The adsorbent surface in an acidic environment is largely protonated, and therefore the chromium anionic groups are attracted stronger by the positively charged adsorbent surface [62]. Also, $\text{pH} < 3$ favor the reduction of Cr(VI) to Cr(III), where most often the reducer is the organic substance and iron present in the adsorbent. However, at $\text{pH} > 5$, no significant adsorption was observed (Fig. 3), due to the competition of HCrO_4^- , $\text{Cr}_2\text{O}_7^{2-}$ and OH^- anions for adsorption sites. Similar results were obtained for adsorption of Cr(VI) on light aggregate [63] and [64].

The sorption of Cr(III) looks different in the function of changing pH. Generally, the amount of adsorbed Cr(III) increases with increasing pH. At $\text{pH} < 4$, the adsorption of Cr(III) is the lowest, above this value it increases as pH rises to about 6. At this value, 89 to 99% of Cr(III) seem to be adsorbed on shales from CM2 and CM3, whereas it is ca. 66% for CM1. However, the sorption can be lower, because of possible precipitation of Cr(III) hydroxide which is likely to form with an increase in pH. The low sorption of Cr(III) in solutions with $\text{pH} < 4$ is probably caused by the increased concentrations of protons which compete with Cr(III) for the adsorbent binding sites [65]. In addition, in acidic solutions, Cr(III) species occur as $\text{Cr}(\text{H}_2\text{O})_6^{3+}$, which are larger by volume, which results from the strong binding of water molecules to cations. This means a limited access of hydrated chromium ions to the adsorbent micropores [61,66], especially those of a slit shape. With an increase in pH, other chromium ion species, for example, CrOH_2^+ , begin to dominate, which attract negatively charged functional groups [61,67]. The gradual increase in pH above 4 also leads to the formation of complex ions and their precipitation in the form of metal hydroxides.

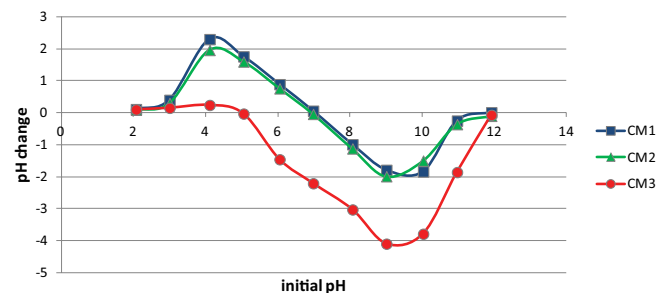


Fig. 2. The zero point of charge results for the shales from coal mines 1, 2 and 3.

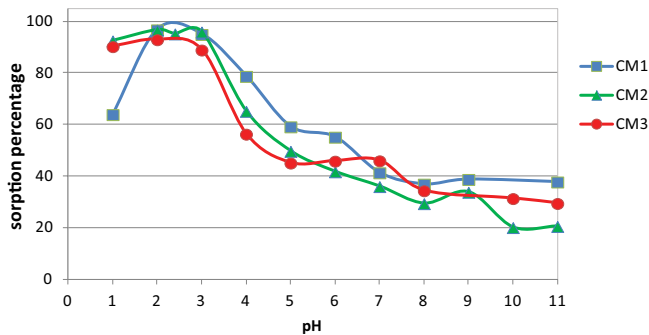


Fig. 3. Effect of pH on Cr(VI) sorption on the shales from coal mines 1, 2 and 3.

3.4. Cr(III) and Cr(VI) sorption isotherms

Based on the performed tests and the calculated amounts of Cr(III) and Cr(VI) adsorbed on the natural shales, the adsorption isotherms were determined (symbols in Figs. 5 and 6).

The adsorption results roughly follow relation $CM2 > CM1 > CM3$ in sorption of both Cr(III) and Cr(VI). The adsorbed amount of Cr(III) ions was 8.25 mg/g for CM2 at the maximum initial concentration, whereas it equaled 6.7 mg/g for CM1 and CM3. These values are better than those reported in works [21] and [28], where 4.12 and 5.03 mg/g were obtained for natural zeolites. In the case of Cr(VI), the maximum sorption was 3.7 mg/g for the sample from CM2, while 2.5 mg/g for CM1 and only 0.5 mg/g for CM3. These results are similar to those given in [34], where 3.31 mg/g was obtained for Cr(VI) sorption on clay. Hence, out of the tested materials, the shale from CM2 has the best adsorptive properties with respect to both Cr(III) and Cr(VI), whereas the shale from CM3 is the weakest adsorbent.

The values of the parameters in the Freundlich, Langmuir, Langmuir–Freundlich, Elovich, Temkin and DR isothermal equations determined from the sorption data are shown in Table 4. The determination coefficients (R^2) range from 0.9080 to 0.9983, with the best fit for the Langmuir–Freundlich isotherm, but only slightly worse for the Langmuir isotherm, then clearly worse for the Freundlich and Elovich isotherm, and relatively weak to the Temkin isotherm. These results indicate that Cr(III) and Cr(VI) sorption does not undergo according to the Temkin isotherm due to rather low R^2 as well as rather high values of uncertainty for A_T (ca. 40%–50%). Hence, the heat of adsorption does not decrease linearly with increasing coverage as assumed in the Temkin isotherm. The Elovich isotherm, although with acceptable R^2 , is characterized by high errors of K_E (31%–158%), and therefore should not be taken into account. The DR isotherm parameters will be commented a few paragraphs below. Out of the tested adsorption models, the Langmuir–Freundlich and Langmuir isotherms give R^2 closest to 1. Although the Langmuir–Freundlich model offers slightly better fit quality, the parameter error estimates are higher than for the Langmuir isotherm, for which they are at a level up to 15%. Therefore, the Langmuir isotherm was presumed the most precise in the studied cases.

In the case of Cr(III), the sorption capacity in the Langmuir model is from 7.67 mg/g (CM1) to 9.85 mg/g (CM3). Values

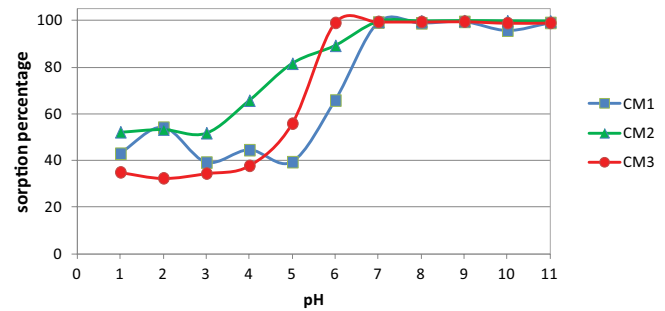


Fig. 4. Effect of pH on Cr(III) sorption on shales from coal mines 1, 2 and 3.

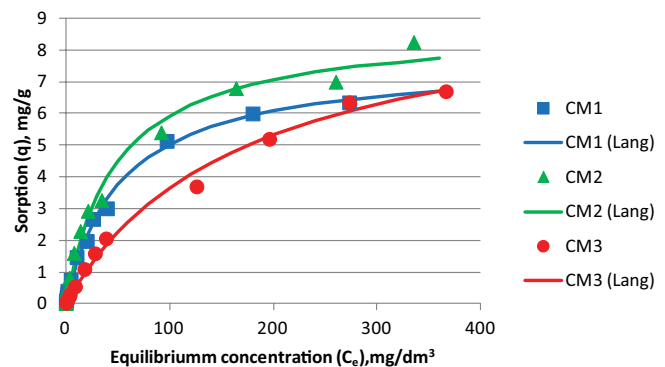


Fig. 5. Cr(III) sorption isotherms on tested samples from coal mines 1, 2 and 3 (symbols - measurement, lines - Langmuir isotherms).

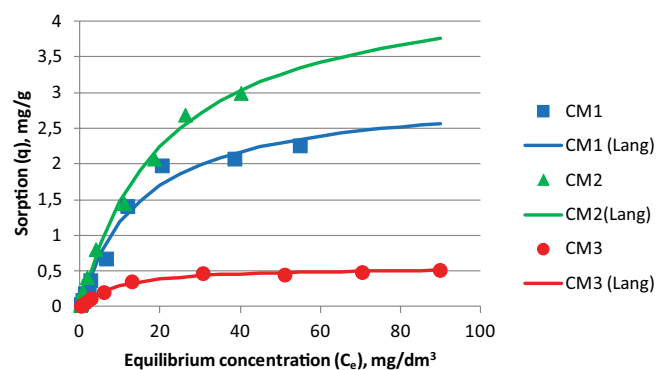


Fig. 6. Cr(VI) sorption isotherms on tested samples from coal mines 1, 2 and 3 (symbols - measurement, lines - Langmuir isotherms).

of K_L indicate that isotherms for CM1 and CM2 have a similar shape, and the isotherm for CM3 reaches saturation for higher values of equilibrium concentration. Indeed, sorption values for CM1 are lower than for other mines, but as the equilibrium concentration increases, these values reach similar values for all mines. Therefore, despite some differences, Q_L values can be considered similar, especially considering the statistically determined error at a level of 3%–7%. In the case of Cr(VI), the determined sorption capacities are significantly lower than for Cr(III) and range from 0.56 mg/g for CM3 to 4.66 mg/g for CM2. As in the case of Cr(III), the CM2 shale manifests highest sorption and the isotherm for CM3

gives the smallest q values in the range of the concentrations considered.

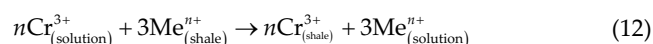
Although the best fit was obtained for the Langmuir–Freundlich and Langmuir isotherms, the Freundlich and Elovich isotherms quite well match the experimental data. This indicates that the shale adsorption is mixed, heterogeneous and nonspecific, which is probably due to the inhomogeneity of the material [47]. The chemical or physical character of sorption is often assessed based on the mean free energy obtained from the DR isotherm. In this case, the energies obtained are from 9.6 to 11.9 kJ/mol, which qualify the sorption as based on ion exchange (8–16 kJ/mol). However, it must be emphasized that DR-based approach requires the knowledge of solubility of the adsorbate in water, which cannot be stated uniquely because of many possible chromium species in the solution. The results given in Table 4 are for $C_s = 810$ g/L for chromium nitrate corresponding to Cr(III), and $C_s = 130$ g/L for potassium dichromate corresponding to Cr(VI). Such values result in very small ratios C_s/C_{DR} so that the isotherms are far from saturation. Consequently, values of Q_{DR} are unlikely large compared to the measured values of q .

A larger share of illite in sample CM2 with a lower content of kaolinite compared to the other samples (Table 1) resulted in better sorption on this sample. The shift of the packet charge from the tetrahedral to octahedral layers in illites is the reason for the greater availability of interpacket spaces for chromium ions than in case of other minerals. The better sorption capacity of this rock compared to samples CM1 and CM3 can be also explained by the increased presence of iron oxides. Iron oxides can form coatings on mineral lamellae, which, on the one hand, can be active surfaces for adsorbed compounds, and on the other hand, prevent access of metal ions to sorption centers [68]. Higher content of kaolinite in samples CM1 and CM3 can also be the reason for weaker Cr(III) sorption, because kaolinite is generally characterized by low sorption capacity for cations.

The sorption results correspond well with the structural properties of the shales (Table 3). The relations $CM2 > CM1 > CM3$ obtained in sorption tests are kept also in structural parameters such as BET surface area and micropore volume obtained via DR equation. It also roughly agrees with fractal dimension which was highest for CM2, although lowest for CM1. The shale from CM2 characterizes also with highest percentage of mesopores (ca. 31%). Hence, it follows the presence of micropores and mesopores increases the BET surface area and the fractal dimension, and affects positively the adsorptive abilities.

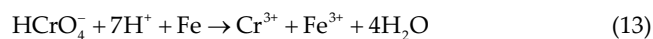
The obtained results indicate that the effectiveness of removing of chromium compounds on raw shales varies between the three mines; and depends on the structure of a given material as well as chemical and mineralogical composition; moreover, it is different for Cr(III) and Cr(VI). The adsorption of Cr(III) ions is much higher compared to the adsorption of Cr(VI) ions under the same conditions. The mechanisms of chromium removal from aqueous solutions are quite complex and not fully understood due to the multitude of factors that may have a significant impact, primarily pH, but also the presence of various functional groups and metals [69]. In the present case, the results obtained from the DR adsorption isotherm suggest that the

main mechanism is associated with ion exchange. This is the most likely Cr(III) removal mechanism. A characteristic feature of clay minerals is their ability to ion exchange, which is conditioned by the presence of unsaturated negative charges located at oxygen atoms and –OH groups at the discontinuities of crystal lattice of minerals (on the crystallite edges) that are compensated by alkali metal cations. Therefore, sorption of transition metals such as Cr(III) is accomplished by ion exchange, which can be represented as follows [70]:



where Me^{n+} is metal ion (K^+ , Na^+ , Ca^{2+} , Mg^{2+} , Mn^{2+}), and n is its valence. The course of ion exchange is strongly influenced by the pH of the environment. At low pH the surface of the shale is positively charged, hence cationic forms of Cr(III) are repelled from the surface and the adsorption is weak. With an increase in pH the surface becomes less positive and the repulsive interactions are weaker, which increases sorption. A further increase in pH above the isoelectric point (pH_{zpc}) charges the surface negatively, which would be beneficial for adsorption of Cr(III) cationic forms. However, at pH larger than 5–6 Cr(III) precipitates, often as $Cr(OH)_3$ [69].

In the case of Cr(VI) adsorption the mechanism is different, because at $pH = 5$ Cr(VI) occurs as anions, mainly $HCrO_4^-$ and $Cr_2O_7^{2-}$ [60]. The anions are attracted by positively charged surface via electrostatic forces. The positive charge of the shale surface can result both from metal cations as mentioned above as well as from protonated functional groups like $-OH_2^+$, which are likely to be formed in acidic environment. A protonated functional group can then reduce Cr(VI) to Cr(III), especially in presence of iron, for example, [71]:



Then a part of Cr(III) can be removed in the way described above, and certain part of Cr(III) is likely to precipitate as $Cr_xFe_{1-x}(OH)_3$ or $Cr_xFe_{1-x}(OOH)$, where $x < 1$ [72].

Figs. 7 and 8 show the sorption percentage vs. initial concentration of chromium ions for Cr(III) and Cr(VI), respectively. In general, the percentage is highest for the lowest initial concentrations and lowers with an increase in the concentration. In the case of Cr(III), it reaches 80%–91% for the shales from CM1 and CM2, and ca. 60% for CM3. As for Cr(VI), the percentage equals 75%–90% for CM1 and CM2 shales, whereas it is only 40%–45% for CM3 shale. Hence, it follows that the shale from CM3 is a rather poor sorbent, while the material from CM1 and CM2 can be assumed good.

3.5. Comparison with other similar adsorbents

Table 5 presents comparison of adsorptive capabilities of the studied shales and other adsorbents of similar origin. Although the studied shales cannot equal with synthetic or modified adsorbents, like synthetic zeolite or activated carbon from Tuñçbilek lignite, or some natural adsorbents, like bentonite or palygorskite clay, their adsorptive capabilities are comparable or better than many other natural adsorbents, including natural zeolite, kaolin or vesicular basalt

Table 4

Parameters of the Freundlich, Langmuir, Langmuir–Freundlich, Elovich, Temkin and Dubinin–Radushkevich isotherms for Cr(III) and Cr(VI) sorption on the tested shales

Parameter	Unit	Cr(III)			Cr(VI)		
		CM1	CM2	CM3	CM1	CM2	CM3
Freundlich isotherm – Eq. (6)							
K_F	mg/g (L/mg) ^{1/n_F}	0.526	0.725	0.208	0.310	0.359	0.101
δK_F^*	%	17	13	16	26	12	23
n_F	–	2.17	2.37	1.67	1.91	1.69	2.62
δn_F^*	%	7	6	5	14	6	16
R^2	–	0.9864	0.9925	0.9952	0.9685	0.9956	0.9736
Langmuir isotherm – Eq. (7)							
K_L	L/mg	0.0190	0.0210	0.0059	0.0649	0.0463	0.1093
δK_L^*	%	7	12	14	22	15	13
Q_L	mg/g	7.67	8.75	9.88	3.00	4.66	0.56
δQ_L^*	%	3	4	6	8	7	3
R^2	–	0.9980	0.9947	0.9967	0.9904	0.9973	0.9967
Langmuir–Freundlich isotherm – Eq. (8)							
K_{LF}	L/mg	0.0160	0.0085	0.0025	0.1016	0.0234	0.1333
δK_{LF}^*	%	19	41	58	15	62	11
Q_{LF}	mg/g	8.19	11.80	14.35	2.45	6.31	0.52
δQ_{LF}^*	%	7	13	25	7	27	4
n_{LF}	–	0.911	0.698	0.807	1.47	0.825	1.27
δn_{LF}^*	%	8	10	10	15	12	11
R^2	–	0.9983	0.9977	0.9978	0.9947	0.9980	0.9980
Elovich isotherm – Eq. (9)							
K_E	L/mg	0.452	0.062	0.013	4.988	0.121	10.81
δK_E^*	%	63	45	33	117	39	158
Q_E	mg/g	1.814	3.667	5.412	0.543	2.340	0.099
δQ_E^*	%	14	15	15	23	18	26
R^2	–	0.9870	0.9826	0.9928	0.9729	0.9923	0.9611
Temkin isotherm – Eq. (10)							
K_T	mg/g	0.911	0.915	1.017	0.471	0.434	0.096
δK_T^*	%	12	12	14	12	16	8
A_T	L/mg	1.317	3.197	0.517	1.632	5.967	2.288
δA_T^*	%	39	52	41	32	54	26
R^2	–	0.9324	0.9214	0.9080	0.9517	0.9164	0.9843
Dubinin–Radushkevich isotherm – Eqs. (3) and (11)							
Q_{DR}	mg/g	30.6	30.4	47.3	13.5	23.3	1.67
δQ_{DR}^*	%	11	7	9	27	12	19
K_{DR}	mmol ² /kJ ²	3,962	3,641	5,439	4,743	5,199	3,512
δK_{DR}^*	%	6	4	4	13	5	14
E_{DR}	kJ/mol	11.2	11.7	9.6	10.3	9.8	11.9
δE_{DR}^*	%	3	2	2	7	3	7
R^2	–	0.9927	0.9964	0.9974	0.9764	0.9973	0.9817

* δy is the standard percentage error for y .

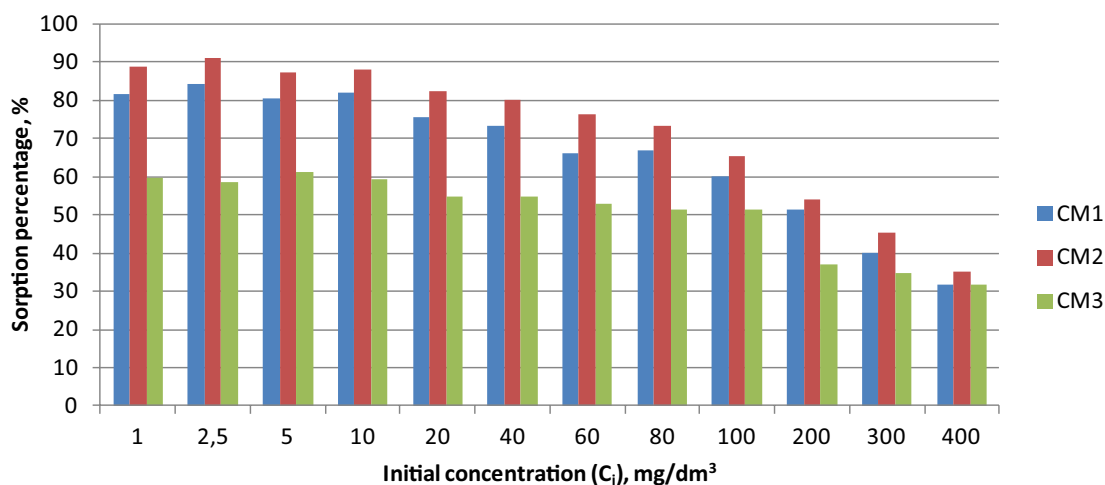


Fig. 7. Sorption percentage on shales from coal mines 1, 2 and 3 vs. initial concentration of Cr(III) ions.

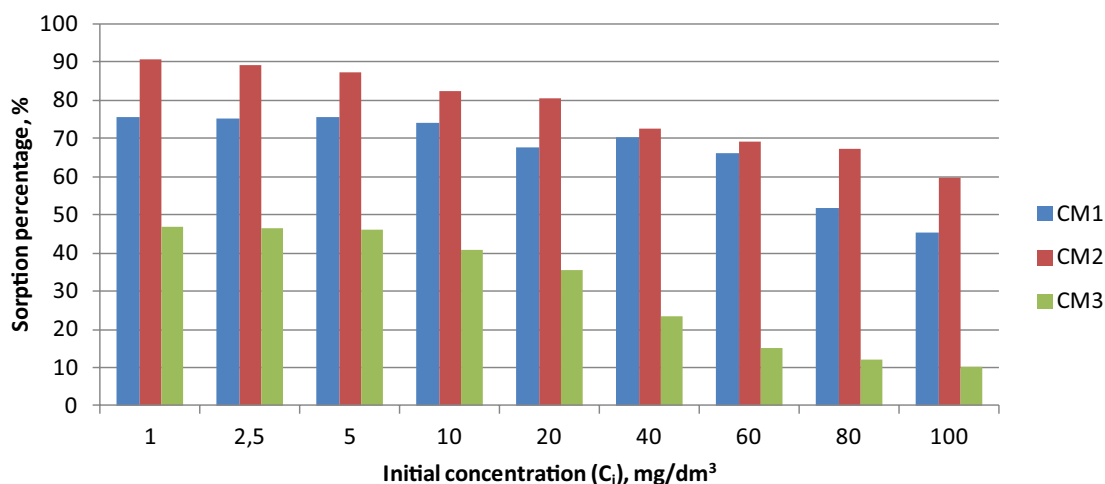


Fig. 8. Sorption percentage on shales from coal mines 1, 2 and 3 vs. initial concentration of Cr(VI) ions.

rock. Table 6 shows costs of several mineral adsorbents. It follows that the considered shale is a mining waste of very low price. Hence, its use as a low-cost adsorbent is economically justified.

4. Conclusions

The shale taken from three coal mines showed different sorption tendencies. It can be concluded the following:

- Out of the tested samples, the best adsorptive properties with respect both Cr(III) and Cr(VI) are observed for shale from coal mine 2, which can be explained by presence of illites and iron oxides as well as by structural and surface properties of the shales.
- The chromium sorption on the tested shales is best explained by the Langmuir–Freundlich, Langmuir and Freundlich isotherms; this indicates a monolayer sorption on heterogeneous surface. The suggested sorption mechanism is ion-exchange.
- The adsorption of chromium compounds depends on the pH of the solution. The highest Cr(VI) adsorption was observed for pH = 4–5, whereas the adsorption of Cr(III) increased with increasing pH from 3 to 6.
- The values of structural and surface parameters are in good agreement with sorption results; in particular, the shale with the highest BET specific surface area, micropore and mesopore content and fractal dimension was the best chromium adsorbent.
- The sorption percentage on the tested materials is 75%–90% for low concentrations of Cr(III) and Cr(VI) ions, whereas it decreases with an increase in chromium concentration. The degree of reduction of Cr(III) concentration from solution on shales was 30%–91%, whereas it was 10%–90% for Cr(VI).
- The tested waste rocks could be used as inexpensive adsorbents for removing chromium compounds from aqueous solutions. They could also be used as protective barriers against infiltration of solutions containing other harmful metal ions.

Table 5
Adsorptive capabilities of selected adsorbents with respect to Cr(III) and Cr(VI)

Adsorbent	Dosage	pH	Initial concentration C_i	Maximum uptake q_{\max}	Adsorption capacity (Langmuir isotherm Q_L)	Reference
	g/L					
Cr(III)						
Shale	20	4	1–500	6.35–8.25	7.67–9.88	This study
Natural zeolite	10	4	10–200	~4	4.12	[21]
Synthetic zeolite	2.5	4	10–200	~42	43.6	[21]
Zeolite	1–25	6.5	1–50	~4	5.03	[28]
Vesicular basalt rock	50	6	20–100	0.36–0.98	0.91	[29]
Kaolin	25	4.5	20–300	~0.9	1.018	[35]
Bentonite	10	2.4	20–200	–	49.75	[37]
Fly ash	10	5	5–50	1.8	2.50	[27]
Cr(VI)						
Shale	20	5	1–100	0.52–3.00	0.56–4.66	This study
Vesicular basalt rock	50	2	0.1–5	0.002–0.079	0.104	[30]
Volcanic pumice	10–100	2	0.5–10	0.004–0.036	0.046	[31]
Volcanic scoria	10–100	2	0.5–10	0.004–0.027	0.045	[31]
Kaolinite	2	4.6	10–250	6.1	11.6	[32]
Clay (treated)	20	2.5	5–30	0.2–1.4	3.31–3.56	[34]
Kaolin	25	4.5	20–200	~0.85	0.878	[35]
Palygorskite clay	1–5	7	20–100	~8–~48	58.48	[36]
Riverbed sand	20	2.5	1.05–7.84	0.04	0.15	[73]
Physically activated carbon from Tunçbilek lignite	–	2	25–1,200	20.59–22.96	23.9–27.6	[18]
Chemically activated carbon from Tunçbilek lignite	–	2	25–1,200	16.78–22.06	21.3–29.0	[18]

Table 6
Price of selected mineral adsorbents

Adsorbent	Price*, EUR/Mg	Reference
Post-mining waste with shale	3	[74]
Sodium bentonite	160	[75]
Diatomite	11,630	[76]
Lignite overburden clays	3	[77]
Zeolite-clinoptilolite	11,600	[78]
Activated carbon	3,490	[79]

* Original prices in PLN were converted to approximate prices in EUR

Symbols

C	– Constant in BET equation
C_e	– Equilibrium concentration of adsorbate, mg/L
C_i	– Initial concentration of adsorbate, mg/L
C_s	– Solubility, g/L
D	– Fractal dimension
E_{DR}	– Free energy in Dubinin–Radushkevich adsorption isotherm, kJ/mol
K_{DR}	– Constant in the Dubinin–Radushkevich equation

$K_{E'} Q_E$	– Parameters in Elovich isotherm
$K_F n_F$	– Parameters in Freundlich isotherm
$K_L Q_L$	– Parameters in Langmuir isotherm
$K_{LF} Q_{LF} n_{LF}$	– Parameters in Langmuir–Freundlich isotherm
$K_T A_T$	– Parameters in Temkin isotherm
m	– Mass of adsorbent, g
n	– Number of layers accessible for adsorption in the modified BET equation
q	– Amount of adsorbate per amount of adsorbent, mg/g
R^2	– Determination coefficient in curve fitting
r_K	– The Kelvin radius corresponding to relative pressure x , nm
S_{BET}	– BET specific surface area, m ² /g
V	– Volume of solution in sorption, L
V_0	– Total volume of micropores in the Dubinin–Radushkevich equation, mm ³ /g
V_{mic}	– Volume of filled micropores at relative pressure x , mm ³ /g
v	– Volume of adsorbed nitrogen at relative pressure x , cm ³ /g, STP
v_m	– Monolayer volume in BET equation, cm ³ /g, STP
v_{\max}	– Maximum volume of adsorbed nitrogen, cm ³ /g, STP

- x — Relative pressure of nitrogen vapor
 δy — Percentage standard error in determination of y

Acknowledgement

The scientific research was funded by the statute subvention of Czestochowa University of Technology, Faculty of Infrastructure and Environment.

References

- [1] USGS, Mineral Commodity Summaries, Chromium Statistics and Information, U.S. Geological Survey, February 2019. Available at: <https://www.usgs.gov/centers/nmic/chromium-statistics-and-information> (accessed on 2019.11.18).
- [2] A. Bielański, Foundations of Inorganic Chemistry, Vol. 2, Polish Scientific Publishers PWN, Warsaw, 2002 (in Polish).
- [3] B. Bartkiewicz, Treatment of Industrial Wastewater, Polish Scientific Publishers PWN, Warsaw, 2002 (in Polish).
- [4] J.H. Zhang, Y.N. Xu, Y.G. Wu, S.H. Hu, Y.J. Zhang, Dynamic characteristics of heavy metal accumulation in the farmland soil over Xiaqingling gold-mining region, Shaanxi, China, *Environ. Earth Sci.*, 78 (2019), <https://doi.org/10.1007/s12665-018-8013-2>.
- [5] H.Q. Wu, Q.P. Wu, J.M. Zhang, Q.H. Gu, L.T. Wei, W.P. Guo, M.H. He, Chromium ion removal from raw water by magnetic iron composites and *Shewanella oneidensis* MR-1, *Sci. Rep.*, 9 (2019) 3687.
- [6] J.R. Dojlido, Chemistry of Surface Waters, Economy and Environment Publishers, Białystok, 1995 (in Polish).
- [7] International Agency for Research on Cancer (IARC), IARC Monographs on the Evaluation of Carcinogenic Risks to Humans: Overall Evaluation of Carcinogenicity, An Updating of IARC Monographs, Vol. 1–42, Supplement 7, WHO, Lyon, 1987.
- [8] K.K. Krishnani, S. Ayyappan, Heavy metals remediation of water using plants and lignocellulosic agrowastes, *Rev. Environ. Contam. Toxicol.*, 188 (2006) 59–84.
- [9] C.E. Barrera-Díaz, V. Lugo-Lugo, B. Bilyeu, A review of chemical, electrochemical and biological methods for aqueous Cr(VI) reduction, *J. Hazard. Mater.*, 223–224 (2012) 1–12.
- [10] S.J. Wu, F.G. Fu, Z.H. Cheng, B. Tang, Removal of Cr(VI) from wastewater by FeOOH supported on Amberlite IR120 resin, *Desal. Water Treat.*, 57 (2016) 17767–17773.
- [11] K. Anarakdim, M. Matos, O. Senhadji-Keblache, M. Benamor, Optimization of hexavalent chromium removal by emulsion liquid membrane (ELM) using sunflower oil as eco-friendly solvent, *Desal. Water Treat.*, 72 (2017) 281–289.
- [12] S. Sadeghi, M.R.A. Moghaddam, M. Arami, Improvement of electrocoagulation process on hexavalent chromium removal with the use of polyaluminum chloride as coagulant, *Desal. Water Treat.*, 52 (2014) 4818–4829.
- [13] J. Lach, Chromium adsorption from waters of different chemical composition, *Inżynieria i Ochrona Środowiska*, 19 (2016) 353–362 (in Polish).
- [14] G. Crini, E. Lichtfouse, Advantages and disadvantages of techniques used for wastewater treatment, *Environ. Chem. Lett.*, 17 (2019) 145–155.
- [15] V.K. Gupta, A. Rastogi, Sorption and desorption studies of chromium (VI) from nonviable cyanobacterium *Nostoc muscorum* biomass, *J. Hazard. Mater.*, 154 (2008) 347–354.
- [16] M.N. Sahmoune, K. Louhab, A. Boukhar, Advanced biosorbents materials for removal of chromium from water and wastewaters, *Environ. Prog. Sustainable Energy*, 30 (2011) 284–293.
- [17] N.A. Kabbashi, A.H. Nour, M. Al-Khatib, M.A. Maleque, Removal of Chromium with CNT Coated Activated Carbon for Waste Water Treatment, Reference Module in Materials Science and Materials Engineering, Elsevier, Amsterdam, 2019.
- [18] A.Y. Orbak, I. Orbak, Effective factor analysis for chromium(VI) removal from aqueous solutions and its application to Tunçbilek lignite using design of experiments, *J. Chem.*, 2019 (2019), <https://doi.org/10.1155/2019/1263735>.
- [19] R. de Abreu Domingos, F.V. da Fonseca, Evaluation of adsorbent and ion exchange resins for removal of organic matter from petroleum refinery wastewaters aiming to increase water reuse, *J. Environ. Manage.*, 214 (2018) 362–369.
- [20] M.S.H. Hashemi, F. Eslami, R. Karimzadeh, Organic contaminants removal from industrial wastewater by CTAB treated synthetic zeolite Y, *J. Environ. Manage.*, 233 (2019) 785–792.
- [21] E. Álvarez-Ayuso, A. García-Sánchez, X. Querol, Purification of metal electroplating waste waters using zeolites, *Water Res.*, 37 (2003) 4855–4862.
- [22] Y. Wu, Y. Zhang, J. Qian, X. Xin, S. Hu, S. Zhang, J. Wei, An exploratory study on low-concentration hexavalent chromium adsorption by Fe(III)-cross-linked chitosan beads, *R. Soc. Open Sci.*, 4 (2017) 170905.
- [23] P.M.B. Chagas, L.B. de Carvalho, A.A. Caetano, F.G.E. Nogueira, A.D. Corrêa, I.R. Guimarães, Nanostructured oxide stabilized by chitosan: hybrid composite as an adsorbent for the removal of chromium (VI), *J. Environ. Chem. Eng.*, 6 (2018) 1008–1019.
- [24] M. Dakiky, M. Khamis, A. Manassra, M. Mer'eb, Selective adsorption of chromium(VI) in industrial wastewater using low-cost abundantly available adsorbents, *Adv. Environ. Res.*, 6 (2002) 533–540.
- [25] S. Nag, A. Mondal, N. Bar, S.K. Das, Biosorption of chromium (VI) from aqueous solutions and ANN modelling, *Environ. Sci. Pollut. Res. Int.*, 23 (2017) 18817–18835.
- [26] M.H. Dehghani, D. Sanaei, I. Ali, A. Bhatnagar, Removal of chromium(VI) from aqueous solution using treated waste newspaper as a low-cost adsorbent: kinetic modeling and isotherm studies, *J. Mol. Liq.*, 215 (2016) 671–679.
- [27] V.K. Gupta, I. Ali, Removal of lead and chromium from wastewater using bagasse fly ash—a sugar industry waste, *J. Colloid Interface Sci.*, 271 (2004) 321–328.
- [28] T.C. Nguyen, P. Loganathan, T.V. Nguyen, S. Vigneswaran, J. Kandasamy, R. Naidu, Simultaneous adsorption of Cd, Cr, Cu, Pb, and Zn by an iron-coated Australian zeolite in batch and fixed-bed column studies, *Chem. Eng. J.*, 270 (2015) 393–404.
- [29] A. Alemu, B. Lemma, N. Gabbiy, Adsorption of chromium (III) from aqueous solution using vesicular basalt rock, *Cogent Environ. Sci.*, 5 (2019) 1650416.
- [30] A. Alemu, B. Lemma, N. Gabbiye, M.T. Alula, M.T. Desta, Removal of chromium (VI) from aqueous solution using vesicular basalt: a potential low cost wastewater treatment system, *Heliyon*, 4 (2018) e00682.
- [31] E. Alemayehu, S. Thiele-Bruhn, B. Lennartz, Adsorption behaviour of Cr(VI) onto macro and micro-vesicular volcanic rocks from water, *Sep. Purif. Technol.*, 78 (2011) 55–61.
- [32] K.G. Bhattacharyya, S.S. Gupta, Adsorption of chromium(VI) from water by clays, *Ind. Eng. Chem. Res.*, 45 (2006) 7232–7240.
- [33] S.S. Gupta, K.G. Bhattacharyya, Adsorption of heavy metals on kaolinite and montmorillonite: a review, *Phys. Chem. Chem. Phys.*, 14 (2012) 6698–6723.
- [34] T.A. Khan, V.V. Singh, Removal of cadmium (II), lead (II), and chromium (VI) ions from aqueous solution using clay, *Toxicol. Environ. Chem.*, 92 (2010) 1435–1446.
- [35] J. Liu, X. Wu, Y. Hu, C. Dai, Q. Peng, D. Liang, Effects of Cu(II) on the adsorption behaviors of Cr(III) and Cr(VI) onto kaolin, *J. Chem.*, 2016 (2016), <https://doi.org/10.1155/2016/3069754>.
- [36] J.H. Potgieter, S.S. Potgieter-Vermaak, P.D. Kalibantonga, Heavy metals removal from solution by palygorskite clay, *Miner. Eng.*, 19 (2006) 463–470.
- [37] S. Tahir, R. Naseem, Removal of Cr(III) from tannery wastewater by adsorption onto bentonite clay, *Sep. Purif. Technol.*, 53 (2007) 312–321.
- [38] J. Wang, Q. Qin, S. Hu, K. Wu, A concrete material with waste coal gangue and fly ash used for farmland drainage in high groundwater level areas, *J. Cleaner Prod.*, 112 (2016) 631–638.
- [39] Z.B. Yu, H.T. Peng, Y.D. Zhu, J. Li, Q. Zhao, M.H. You, X.P. Zhang, Technical Feasibility Study of Unfired Brick with Coal Gangue at the Wulanmulun Site, Inner Mongolia, China, P. Chen, Ed., Material Science and Environmental Engineering, Taylor & Francis Group, London, 2016, pp. 263–266.

- [40] Statistics Poland. Available at: <https://stat.gov.pl/obszary-tematyczne/srodowisko-energia/srodowisko/ochrona-srodowiska-2018,1,19.html> (accessed 30.05.2019).
- [41] Grupa Kapitałowa Lubelski Węgiel Bogdanka, Integrated Report 2017. Available at: https://www.lw.com.pl/file,21938,raport_zintegrowany_20171.pdf (accessed 2019.03.25) (in Polish).
- [42] K. Niedbalska, Using of selected methods of testing the hydrogeological properties of rocks for predicting the impact of open pit reclamation using mining wastes on the condition of groundwater, *Górnictwo Odkrywkowe*, 59 (2018) 39–43 (in Polish).
- [43] L.J. Yu, Y.L. Feng, W. Yan, The current situation of comprehensive utilization of coal gangue in China, *Adv. Mater. Res.*, 524–527 (2012) 915–918.
- [44] B. Jabłońska, A.V. Kityk, M. Busch, P. Huber, The structural and surface properties of natural and modified coal gangue, *J. Environ. Manage.*, 190 (2017) 80–90.
- [45] B. Jabłońska, Sorption of phenol on rock components occurring in mine drainage water sediments, *Int. J. Miner. Process.*, 104–105 (2012) 71–79.
- [46] K.M. Skarżyńska, *Coal Mining Waste and its Use in Civil Engineering*, Agricultural University Publishers, Cracow, 1997 (in Polish).
- [47] B. Jabłońska, E. Siedlecka, Removing heavy metals from wastewaters with use of shales accompanying the coal beds, *J. Environ. Manage.*, 155 (2015) 58–66.
- [48] E. Myślińska, *Laboratoryjne badania gruntów i gleb*, Wyd. Uniwersytetu Warszawskiego, Warszawa, 2010 (in Polish).
- [49] Regulation of the Minister of the Environment of September 9, 2002 on Soil Quality Standards and Soil Quality Standards (Journal of Laws of 2002 No. 165, item 1359) (in Polish).
- [50] F. Rouquerol, J. Rouquerol, K. Sing, *Adsorption by Powders and Porous Solids Principles, Methodology and Applications*, Academic Press, London, 1999.
- [51] F. Wang, S. Li, Determination of the surface fractal dimension for porous media by capillary condensation, *Ind. Eng. Chem. Res.*, 36 (1997) 1598–1602.
- [52] S.S. Tripathy, S.B. Kanungo, Adsorption of Co^{2+} , Ni^{2+} , Cu^{2+} and Zn^{2+} from 0.5M NaCl and major ion sea water on a mixture of $\delta\text{-MnO}_2$ and amorphous FeOOH , *J. Colloid Interface Sci.*, 284 (2005) 30–38.
- [53] ASTM D1687–17, *Standard Test Methods for Chromium in Water*, ASTM International, West Conshohocken, PA, 2017. Available at: www.astm.org.
- [54] O. Hamdaoui, E. Naffrechoux, Modeling of adsorption isotherms of phenol and chlorophenols onto granular activated carbon. Part I. Two-parameter models and equations allowing determination of thermodynamic parameters, *J. Hazard. Mater.*, 147 (2007) 381–394.
- [55] O. Hamdaoui, E. Naffrechoux, Modeling of adsorption isotherms of phenol and chlorophenols onto granular activated carbon. Part II. Models than more than two parameters, *J. Hazard. Mater.*, 147 (2007) 401–411.
- [56] Q. Hu, Z. Zhang, Application of Dubinin–Radushkevich isotherm model at the solid/solution interface: a theoretical analysis, *J. Mol. Liq.*, 277 (2019) 646–648.
- [57] Z. Shang, L.W. Zhang, X. Zhao, S. Liu, D. Li, Removal of Pb(II), Cd(II) and Hg(II) from aqueous solution by mercapto-modified coal gangue, *J. Environ. Manage.*, 231 (2019) 391–396.
- [58] K.G. Bhattacharyya, S.S. Gupta, Adsorption of Fe(III) from water by natural and acid activated clays: studies on equilibrium isotherm, kinetics and thermodynamics of interactions, *Adsorption*, 12 (2006) 185–204.
- [59] M. Thommes, K. Kaneko, A.V. Neimark, J.P. Olivier, F. Rodriguez-Reinoso, J. Rouquerol, K.S.W. Sing, Physisorption of gases, with special reference to the evaluation of surface area and pore size distribution (IUPAC Technical Report), *Pure Appl. Chem.*, 87 (2015) 1051–1069.
- [60] L.K. Cabatingan, R.C. Agapay, J.L.L. Rakels, M. Ottens, L.A.M. van der Wielen, Potential of biosorption for the recovery of chromate in industrial wastewaters, *Ind. Eng. Chem. Res.*, 40 (2001) 2302–2309.
- [61] P. Miretzky, A.F. Cirelli, Cr(VI) and Cr(III) removal from aqueous solution by raw and modified lignocellulosic materials: a review, *J. Hazard. Mater.*, 180 (2010) 1–19.
- [62] M.R. Panuccio, A. Sorgona, M. Rizzo, G. Cacco, Cadmium adsorption on vermiculite, zeolite and pumice: batch experimental studies, *J. Environ. Manage.*, 90 (2009) 364–374.
- [63] E.M. Kalthori, K. Yetilmezsoy, N. Uygur, M. Zarrabi, R.M.A. Shmeis, Modeling of adsorption of toxic chromium on natural and surface modified lightweight expanded clay aggregate (LECA), *Appl. Surf. Sci.*, 287 (2013) 428–442.
- [64] A.R. Rahmani, M. Foroughi, Z.N. Motlagh, S. Adabi, Hexavalent chromium adsorption onto fire clay, *Avicenna J. Environ. Health Eng.*, 3 (2016) 5029.
- [65] D. Kratochvil, P. Pimentel, B. Volesky, Removal of trivalent and hexavalent chromium by seaweed biosorbent, *Environ. Sci. Technol.*, 32 (1998) 2693–2698.
- [66] M. Aoyama, M. Kishino, T.-S. Jo, Biosorption of Cr (VI) on Japanese cedar bark, *Sep. Sci. Technol.*, 39 (2005) 1149–1162.
- [67] J.G. Parsons, M. Hejazi, K.J. Tiemann, J. Henning, J.L. Zarde-Torresdey, An XAS study of the binding of copper(II), zinc(II), chromium(III) and chromium(VI) to hops biomass, *Microchem. J.*, 71 (2002) 211–219.
- [68] J. Kyzioł, *Clay Minerals as Heavy Metal Sorbents*, Zakład Narodowy im. Ossolińskich, Polish Academy of Sciences, Wrocław, 1994 (in Polish).
- [69] V.E. Pakade, N.T. Tavengwa, L.M. Madikizela, Recent advances in hexavalent chromium removal from aqueous solutions by adsorptive methods, *RSC Adv.*, 9 (2019) 26142–26164.
- [70] I. Ghorbel-Abid, A. Jrad, K. Nahdi, M. Trabelsi-Ayadi, Sorption of chromium (III) from aqueous solution using bentonitic clay, *Desalination*, 246 (2009) 595–604.
- [71] S. Fan, Y. Wang, Y. Li, J. Tang, Z. Wang, J. Tang, X. Li, K. Hu, Facile synthesis of tea waste/ Fe_3O_4 nanoparticle composite for hexavalent chromium removal from aqueous solution, *RSC Adv.*, 7 (2017) 7576–7590.
- [72] E. Petala, K. Dimos, A. Douvalis, T. Bakas, J. Tucek, R. Zbořil, M.A. Karakassides, Nanoscale zero-valent iron supported on mesoporous silica: characterization and reactivity for Cr(VI) removal from aqueous solution, *J. Hazard. Mater.*, 261 (2013) 295–306.
- [73] Y.C. Sharma, C.H. Weng, Removal of chromium(VI) from water and wastewater by using riverbed sand: kinetic and equilibrium studies, *J. Hazard. Mater.*, 142 (2007) 449–454.
- [74] J. Kulczycka, R. Uberman, M. Cholewa, Analiza kosztów i korzyści zagospodarowania odpadów z górnictwa węgla kamiennego, *Studia Ekonomiczne*, 166 (2014) 272–282.
- [75] www.technologie-budowlane.com/Granulat_hydroizolacyjny_SS100__WATERSTOPPAGE-3-346-9_31_18-.html (accessed on December 7, 2019).
- [76] <https://biogo.pl/pl/p/ZIEMIA-OKRZEMKOWA-AMORFICZNA-DIATOMIT-1-kg-WIADERKO-PERMA-GUARD/21572> (accessed on December 7, 2019).
- [77] <https://kwbbelchatow.pgegiel.pl/Oferta/Kopaliny-i-kruszywa> (accessed on December 7, 2019).
- [78] https://www.magicznyogrod.pl/zeolit-_klinoptylolit.html (accessed on December 7, 2019).
- [79] <http://water-house.pl/z%20C5%82o%20C5%BCa-filtracyjne/509-w%20C4%99giel-aktywny-1kg.html> (accessed on December 7, 2019).